HHS Public Access

Author manuscript

Cancer Res. Author manuscript; available in PMC 2020 February 15.

Published in final edited form as:

Cancer Res. 2019 August 15; 79(16): 4099–4112. doi:10.1158/0008-5472.CAN-18-4075.

Recycling endosomes in mature epithelia restrain tumorigenic signaling

Luca D'Agostino[1,*], **Yingchao Nie**[2,*], **Sayantani Goswami**[1,*], **Kevin Tong**[3], **Shiyan Yu**[1], **Sheila Bandyopadhyay**[1], **Juan Flores**[1], **Xiao Zhang**[1], **Iyshwarya Balasubramanian**[1], **Ivor Joseph**[1], **Ryotaro Sakamori**[1], **Victoria Farrell**[1], **Qi Li**[2], **Chung S. Yang**[4], **Bin Gao**[5], **Ronaldo P. Ferraris**[6], **Ghassan Yehia**[7], **Edward M. Bonder**[1], **James R. Goldenring**[8], **Michael P. Verzi**[3,9], **Lanjing Zhang**[1,4,9,10], **Y. Tony Ip**[2,#], **Nan Gao**[1,9,#]

[1]Department of Biological Sciences, Rutgers University, Newark, NJ, 07102, USA

[2]Program in Molecular Medicine, University of Massachusetts Medical School, Worcester, MA, 01605, USA

[3]Department of Genetics, Rutgers University, Piscataway, NJ, 08854, USA

[4]Department of Chemical Biology, Ernest Mario School of Pharmacy, Rutgers University, Piscataway, NJ, 08854, USA

[5]Department of Internal Medicine, Taixing Chinese Medicine Hospital, Taixing, Jiangsu, 225400, China

[6]Department of Pharmacology, Physiology, and Neuroscience, Rutgers New Jersey Medical School, Newark, NJ, 07103, USA

[7]Rutgers Genome Editing Core Facility, Rutgers University, New Brunswick, NJ, 08903, USA

[8]Department of Surgery, Cell and Developmental Biology, and Epithelial Center, Vanderbilt University School of Medicine, Nashville, TN, 37232, USA

[9]Rutgers Cancer Institute of New Jersey, New Brunswick, NJ, 08903, USA

[10]Department of Pathology, Princeton Medical Center, Plainsboro, NJ 08536, USA

Abstract

The effects of polarized membrane trafficking in mature epithelial tissue on cell growth and cancer progression have not been fully explored in vivo. A majority of colorectal cancers have reduced and mislocalized Rab11, a small GTPase dedicated to trafficking of recycling endosomes. Patients with low Rab11 protein expression have poor survival rates. Using genetic models across species, we show that intact recycling endosome function restrains aberrant epithelial growth elicited by APC or RAS mutations. Loss of Rab11 protein led to epithelial dysplasia in early animal development and synergized with oncogenic pathways to accelerate tumor progression initiated by carcinogen, genetic mutation, or aging. Transcriptomic analysis uncovered an immediate

[#]**Corresponding Authors:** Tony Ip, Ph.D.: tony.ip@umassmed.edu; Nan Gao, Ph.D.: ngao@rutgers.edu.
[*]These authors contributed equally to this work.

The authors declare no potential conflicts of interest.

expansion of the intestinal stem cell pool along with cell-autonomous Yki/Yap activation following disruption of Rab11a-mediated recycling endosomes. Intestinal tumors lacking Rab11a traffic exhibited marked elevation of nuclear Yap, upd3/IL6-Stat3, and amphiregulin-MAPK signaling, while suppression of Yki/Yap or upd3/IL6 reduced gut epithelial dysplasia and hyperplasia. Examination of Rab11a function in enteroids or cultured cell lines suggested that this endosome unit is required for suppression of the Yap pathway by Hippo kinases. Thus, recycling endosomes in mature epithelia constitute key tumor suppressors, loss of which accelerates carcinogenesis.

INTRODUCTION

The initiation and progression of the vast majority of epithelial neoplasia involve expansion of tumor cell mass and concurrent dysplastic organization, exemplified by loss of cell polarity, of the neoplastic glands. Typically, dysplasia precedes development of advanced invasive carcinoma in most epithelial organs, including the colon (1–3). Whether the structural changes in tissue morphology solely reflect disease progression initiated by oncogenic drivers remains a matter for debate. To date, there is a scarcity of available data examining whether a disruption of cell polarity cues, not linked to known oncogenic drivers, may also constitute an unrecognized pathway to neoplastic development. Mounting cancer research literature has focused on cellular processes directly related to cell proliferation and apoptosis, research linking impaired intracellular trafficking governing epithelial polarity to tumor initiation/progression remains underexplored (4).

Apical-basolateral cell polarity manifested by columnar epithelial organization is maintained by membrane trafficking regulators, in particular the Rab small GTPases. Among the diverse intracellular trafficking organelles, recycling endosomes represents a hallmark structure in mature glandular epithelial cells (5). The recycling endosome compartment is composed of a heterogeneous collection of tubule-vesicular membrane compartments that sort and deliver plasma membrane constituents. The evolutionarily conserved Rab11 family of small GTPases are dedicated recycling endosome resident proteins that execute the canonical sorting functions of this compartment. *Drosophila* has a single *Rab11 gene* and zygotic homozygous Rab11 mutants are lethal (6). In *Drosophila* egg chamber, Rab11 maintains junctions between germ and niche cap cells (7), and appears to impact cellular turnover and differentiation (8). Humans and mice have three Rab11 family members, *Rab11a, Rab11b, and Rab25*. In developing mouse gut, differentiated intestinal epithelial cells express high levels of *Rab11a*, whereas epithelia with an impaired apical-basolateral polarity showed a reduction in Rab11a expression (9). *Rab11a*$^{-/-}$ mice die in early fetal stage (10). In both *Drosophila* midgut and mouse intestine, epithelial cell-specific ablation of *Rab11 (Rab11a* in mice*)* caused epithelial hyperplasia accompanied by an elevated production of pro-inflammatory cytokines (11). Loss of *Rab11a* in intestinal epithelial cells (IECs) disturbs apical membrane morphogenesis and apical transport of cargo essential for mature enterocyte's structure and function (12,13). In addition, when *Rab11a* was acutely removed from mouse IECs via CreER, a rapid induction of abnormal apical membrane structures was ectopically formed along the basolateral domain (13). Thus, genetic, developmental, and cell biological studies demonstrated the existence of an evolutionarily conserved function of

Rab11 in maintaining intestinal epithelial integrity and polarity *in vivo*. The consequences of Rab11 endosome functionality on cellular growth and long-term gut homeostasis have not been defined.

Here, we show that RAB11 is reduced in a majority of colorectal cancer patient tissue samples, and Rab11a protein deficiency in mice causes early onset of epithelial dysplasia. Using genetic approaches across species, we demonstrate that the integrity of recycling endosome function in mature gut epithelia can counterbalance tumorigenic growth elicited by Ras or APC mutations. Alteration of recycling endosome function synergizes with oncogenic pathways and accelerates carcinogenesis induced by chemical carcinogen, genetic mutation, or aging. Additionally, loss of *Rab11* immediately expands a stem cell pool and cells autonomously activate Yki/Yap. We found that Rab11 endosomes maintain the integrity of LATS kinase activity in part through delivery and assembly of a junctional complex. *Rab11*-deficient tumor cells produce high levels of inflammatory and growth signaling; whereas suppressing either Yki/Yap or upd3/IL6 reduces epithelial dysplasia and hyperplasia. We propose that an important and novel function of Rab11 endosomes in mature epithelia is to confine tumorigenic signaling to appropriate homeostatic levels in order to maintain normal tissue growth and turnover.

MATERIALS AND METHODS

Mice

Rab11a^{flox}, *APC*^{Min}, *Villin-Cre*, and *Villin-CreER* mice have been described previously (please see key resource table in Supplementary Information). A new mouse *Rab11b* knockout allele was generated by single guide (sg)RNA and Cas9 mRNA co-injection into murine zygotes (detailed in Supplementary Methods). All procedures carried out have been approved by Rutgers, IACUC community.

Drosophila stocks and genetics

Fly stocks were maintained at room temperature (approximately 22°C) in yeast extract/cornmeal/molasses/agar food medium. *w*^{1118}, Myo1A-Gal4^{ts} >UAS-GFP or Myo1A-Gal4^{ts} >UAS-GFP X *w*^{1118} flies were used as wild type control in different experiments. Transgenic and RNAi fly stocks were obtained from Vienna Drosophila Research Center (VDRC, labeled as V) or Bloomington Drosophila Stock Center (labeled as B), or otherwise as cited (14–18). The stocks include Rab11^{S25N} dominant negative (B9792), Rab11 RNAi (RNAi1: V108382, RNAi2: B27730), UAS-EGFR$^{Act\ (A887T)}$ (B9533), UAS-Ras^{v12} (B64195), *msn* TRiP RNAi (B28791), UAS-Wg-HA (B108487), APC RNAi (RNAi1:V110290, RNAi2: V51468), Yki RNAi (B31965), YkiN+C RNAi (gift from J. Jiang, UT Southwestern), *upd3* mutant (17), UAS-Yki-act (18). For transgenic expression of UAS-dsRNA or -cDNA constructs, newly enclosed flies were kept in vials with regular food medium at room temperature until 5-8 days old, and were shifted to 29 °C for 1-5 days as indicated in the individual figures for optimal results to inactivate the tubulin-Gal80^{ts} repressor and to enable Gal4 dependent UAS-dsRNA or transgene expression. Female flies were used for tissue dissection for various assays including immunofluorescence staining and RNA isolation for quantitative PCR.

Kaplan Meier survival analysis

The following data of all colorectal cancer cases in the TCGA using cBioportal were extracted: RAB11A mRNA levels, intervals between the times of last follow-up and diagnosis, statuses of all-cause death (for overall survival) and disease-free (for disease-free survival), tumor stage, and patient sample ID. The patients who were deemed lost to the follow-up was censored in the survival analyses, which were conducted using the Cox regression model of the Stata (version 14, Stata Corp, College Station, TX, USA) and adjusted for tumor stage. We conducted a step-wise search for the best cutoff of RAB11A mRNA level ((RNA Seq V2 RSEM), using 5 and 10 percentiles. The 5-percentile was chosen for its smallest p value (the most statistical significance). We compared cases of the low mRNA expression level (the lower 5 percentile, N=16) to those (between 5 and 95 percentiles) as reference (N=298), and those of the highest 5 percentile (N=17). The regression data shown were those of multivariate Cox regression, including age, tumor stage and sex as the covariates. A $p<0.05$ was considered statistically significant.

RAB11A immunohistochemistry using human colon cancer tissue microarray

Human Tissue Microarray for colon cancer BC051110a comprised of 110 human colon cancer tissue core samples (Stage I: 4, II: 71, III: 28, and IV: 7; Grade I: 41, II: 46, and III: 23) and 10 human normal colon core samples was purchased from US BioMax, Inc. The tissue microarray was processed for immunohistochemical analysis using a primary rabbit anti-Rab11a antibody (1:500, US Biologicals, R0009). Immunohistochemistry signals of RAB11A were quantified using the NIH Image J with an IHC toolbox package plugin designed for DAB-chromogenic IHC. Three colonic epithelial glands (normal or tumorous) from each of the 120-sample array were manually circled as Region of Interest and individually measured for DAB signals. An average value for each sample was then obtained. After ranking, the sample with the medium value was identified and used to calculate the fold changes for the remaining samples. A graph plotting the fold changes according the medium value ($\log_{10}$) was generated. A Mann-Whitney U test showed significant difference ($p<0.001$) between the normal and colon cancer samples. For RAB11A and YAP immunohistochemistry on colon cancer sections, serial sections (thickness of 4 micrometers) of 13 colon tumor samples (3 tubulovillous adenoma, 1 stage I, 2 stage II, 5 stage III, and 2 stage IV CRC) with adjacent normal colon mucosa were selected from the tissue bank of University Hospital at Princeton, New Jersey.

RNA isolation, sequencing, and GSEA analysis for mouse intestinal tissues

At 3 months of age, $Rab11a^{FL/FL}$ (no CreER), $Rab11a^{FL/FL}$; Villin-CreER, $Rab11a^{FL/FL}$; $Rab11b^{-/-}$; Villin-CreER, and $Rab11b^{-/-}$ mice (n=3 for each genotype), were intraperitoneally injected with 200 μl of tamoxifen (20 mg/ml) dissolved in corn oil. Two days after tamoxifen injection, mouse jejunum was collected and immediately snap frozen in liquid nitrogen. 2-3 mm of frozen jejunum was then processed for RNA isolation. Tissues were immersed in 800 μl of Buffer RLT (provided by Qiangen RNeasy Plus Mini Kit, 74134) with 10 μM β-Mercaptoethanol, homogenized by passing tissue/lysate through a 20-gauge needle (BD, 305176) for 20 times on ice. The remaining isolation procedure was

completed as outlined in the Qiagen RNeasy mini protocol. RNA was eluted from spin column using 30 μl of RNase free water. Quality of RNA was assessed by a bioanalyzer.

RNA was sequenced using Illumina's TruSeq RNA Library Prep kit v2. RNA reads were processed using HISAT2 (v2.1.0) using the Rutgers University Amarel High Performance Computing Cluster. Aligned files were run together using StringTie (v1.3.4) and analyzed using DESeq2 (Release 3.7) to normalize Fragments per Million (FPM) values using default settings and expression was visualized using heatmaps. For differential gene expression analysis, genes were pre-ranked based on signed P-value, where sign is based on logFC from DESeq2. Pre-ranked gene lists were then analyzed against select gene lists of interest to determine significance of differential expression between conditions using GSEA. 1000 permutations were performed for each gene list tested, and normalized enrichment scores (NES) and p values are reported for Lgr5 intestinal stem cell genes, and differentiation genes signatures based on Gene Ontology Terms.

Transcriptomic analysis of *Drosophila* Rab11 RNAi midgut

Total RNA was extracted from 20 guts of flies from Myo1A^{ts} >GFP control and >*Rab11* RNAi (V108382), respectively. The flies were shifted to 29°C for 5 days before dissection. Three independent biological samples were used for total RNA isolation The RNA was sequenced using either the Applied Biosystems' Ion Torrent platform (PrimBio). Fastqc (version 0.10.1) (http://www.bioinformatics.babraham.ac.uk/projects/fastqc) was used on the fastq sequences for all six samples (3 control and 3 Rab11 RNAi) to generate sequence quality reports. The raw sequences were mapped to the reference genome Drosophila melanogaster Ensembl BDGP5 using the aligner STAR (version 2.4.2a). HTseq-count (version 0.6.1) was used to count uniquely mapped reads at the gene level. DESEQ2 was used to perform statistical analysis to determine differentially expressed genes between the control samples and the knockdown samples. Expression of Rab11 and Upd3 were validated using the IGV tool (version 2.3.60). Differentially expressed genes are those with Padj value < 0.05 (N = 2018). The differentially expressed genes were used for the pathway analysis using Enrichr. The RNA sequencing data can be accessed from GEO (accession number GSE92705). The GSEA analysis on fly gut RNA-Seq data was conducted using GSEA (v3.0: build 0160, Broad Institute, Massachusetts Institute of Technology, Cambridge, MA) as described before. The flybase.org was used to convert YAP related mammalian genes to fly orthologs with a matching score greater than 3. The list of fly genes used for the analysis are below: unpg, ImpL2, vg, upd3, Cdc6, mys, tld, Actbeta, Gadd45, kibra, Det, cv-c, tj, tok, Cdk4, sd, Fs, maf-S, fz, CycD, Ephrin, phtf, dpp, TRAM, pk, chico, Lim3, ci, Ccn, esn. The following parameters were set for the GSEA, including 1000 for number of permutations, phenotype for permutation type, weighted for enrichment statistic, Signal2Noise for Metric for ranking genes, real for gene list sorting mode, descending for gene list ordering mode, meandiv for normalization mode, no_balance for randomization mode and timestamp for seed for permutation.

Quantification and Statistical Analysis

Statistical and graphic data analyses were conducted using Prism GraphPad 7.04 (https://www.graphpad.com) and Microsoft Excel 2016. The experimental results were reported

from 3 to 6 mice of each genotype unless a specific number was described in the main text and figure legends. Bar graphs are presented as mean ± S.E.M. Box-and-whisker plots show mean and 10-90 percentile with outliners represented as dots. *P*-values are labeled on individual graphs with $p<0.05$ considered as statistically significant. **See** additional methods in Supplementary Information.

RESULTS

Analysis of RAB11 deficiency on mouse intestinal tumorigenesis and survival

From birth, specific knockout of Rab11a in mouse IECs (*Rab11a*$^{\Delta IEC}$) resulted in crypt hyperproliferation (Suppl. Fig. 1A) and low-grade dysplasia (Suppl. Fig. 1B, C) throughout the small intestine (also see Ref. (11). At 150 days, all *Rab11a*$^{\Delta IEC}$ mice exhibited irregular cribriform proliferation in villi (Suppl. Fig. 1D). At one year, the distal intestines of ~30% of *Rab11a*$^{\Delta IEC}$ mice developed 2-3 well-demarcated tubular adenomas (**box 1**, Fig. 1A) and high-grade dysplasia (**box 2**, Fig. 1A) that exhibited complex glandular (cribriforming) structures, marked nuclear pleiomorphism, necrosis, and increased mitotic activities (Fig. 1A). Such dysplastic lesions were not observed in wild type littermates suggesting that *Rab11a* deficient animal were predisposed to tumorigenesis during aging.

Rab11a-deficient IECs produced elevated levels of inflammatory cytokines (11) opening the possibility that an inflammatory microenvironment may participate in driving tumor progression. To address this question, the azoxymethane-dextran sulfate sodium (AOM-DSS) model for tumor induction by AOM after inflammatory response elicited by DSS (19) was adopted to study *Rab11a*$^{\Delta IEC}$ mice. As *Rab11a*$^{\Delta IEC}$ mice have higher baseline level of inflammatory cytokines compared to wild-type mice, a single dose of AOM (10 mg/kg body weight) was administered without exposing to DSS (Fig. 1B). After 8 weeks, AOM-treated *Rab11a*$^{\Delta IEC}$ mice showed a higher mortality rate (Fig. 1C), and surviving animals formed 2 to 6 poorly differentiated c-Myc^{+} and BrdU^{+} tubular adenomas in the ileum (Fig. 1D, E, Suppl. Fig. 2A, B). These tumors exhibited complex glandular (cribriforming) structures, marked nuclear pleiomorphism, necrosis, increased mitotic activities, and single infiltrating cells in mucosa; the tumors are best classified as intramucosal carcinoma (Suppl. Fig. 2B). By contrast, AOM treatment did not elicit any intestinal tumors in wild type littermate mice (Fig. 1D). Thus, loss of *Rab11a* functionality and the associated elevated inflammatory response appeared to increase susceptibility to AOM-induced tumorigenesis.

We explored the consequence of loss of *Rab11a* on tumor progression in genetically susceptible mice expressing the *APC*^{Min} driver mutation by comparing *Rab11a*$^{\Delta IEC}$; *APC*^{Min} mice and their *APC*^{Min} littermates having intact *Rab11a* alleles. Two-month old *Rab11a*$^{\Delta IEC}$; *APC*^{Min} mice developed twice the number of adenomas that were 5 times larger and occupied larger epithelial fields as compared to tumor fields in *APC*^{Min} (Fig. 1F–J, Suppl. Fig. 2D). Increased tumor burden was also reflected by a rapid decline of animal health that required termination of the experiments. Compared to larger *APC*^{Min} adenomas (Fig. 1K), pan cytokeratin staining revealed that *Rab11a*$^{\Delta IEC}$; *APC*^{Min} mice had a higher frequency of, horizontally-expansile intramucosal adenomas with micro-invasive features (arrow in Fig. 1L, and Suppl. Fig. 2E).

Analysis of the Oncomine database uncovered a significant reduction of *RAB11A* mRNA level in human colon cancers across 19 independent databases (p=2.7E-11, Fig. 2A). Similarly, normal colonic epithelia had strong and specific Rab11A apical and subapical cytoplasmic immunostained regions (Left panels in Fig. 2B, and Suppl. Fig. 3A), whereas the majority of colon cancers exhibited lower Rab11A levels (Fig. 2B, right panels). This data represents Rab11A levels across 110 human colon cancer tissue samples along with 10 normal colon tissues (Suppl. Fig. 3B). Fifteen percent of the carcinomas exhibited over 2-fold reduction in Rab11A level compared to the median sample (Fig. 2C) and 11 samples with the most reduced Rab11A levels were found to have stage II or more advanced carcinomas (Fig. 2C, D). Within the same tissue samples, areas of colonic adenocarcinoma (Suppl. Fig. 3D, see red dotted region) showed reduced apical Rab11A staining compared to the adjacent normal tissue with strong apical Rab11A localization (Suppl. Fig. 3D, see black lined region). Reduction of apical Rab11A was well correlated with epithelial dysplasia (Suppl. Fig. 3E), as even low-grade tumors displayed significant Rab11A reductions (n=41, p<0.01, Suppl. Fig. 3F). Ten adenocarcinomas (9%) showed higher Rab11A levels than average normal colonic epithelia (Fig. 2C). The trend for reduction of RAB11A expression in colon cancers was also independently observed in 70 human colorectal cancers (Nie et al, UMass, personal correspondence).

Kaplan-Meier survival analysis of 331 colon cancer patients using the TCGA database showed that patients with the most reduced RAB11A mRNA levels (lowest 5 percentile, mean value of 1894.3 within a range of 1626.21 - 2071.2) had a significantly reduced survival rate (p<0.001) than the mid-level group (mean mRNA value of 3404.28 within a range of 2102.26 - 5036.07). By contrast, patients with the most upregulated RAB11A levels (top 5 percentile) do not show a different survival rate (p=0.25, Suppl. Fig. 3G). In addition, examination of a human colon cancer-resembling mouse colonic adenocarcinoma induced by 2-amino-1-methyl-6-phenylimidazo[4,5-b]pyridine (PhIP) (20) revealed a reduction of Rab11 apical localization as compared to adjacent normal glands (Suppl. Fig. 3H). The above results indicate that reduced levels of Rab11 expression is linked to both advanced-stage carcinoma and poorer survival rates.

Rab11 function modulates oncogenic pathways and stem cell pools

In *Drosophila*, zygotic homozygous *Rab11* mutants are lethal (21), consequently a molecular system to spatially and temporally control expression of *Rab11* RNAi in the adult *Drosophila* midgut enterocytes that enabled development of three independent *Rab11* RNAi lines (11). Briefly, a *Myo1A* promoter-Gal4 (Myo1A>) construct in only active in enterocytes but not in intestinal stem cells (ISCs) or enteroblasts (EBs) (16). A Myo1Ats> (tubulin promoter-Gal80ts) construct acts as a temperature sensitive repressor of Gal4 that in turn provides temporal control of *UAS-Rab11 RNAi* constructs, as well as the expression of the UAS-dependent mCD8GFP reporter (15,16). Midguts stained for phosphorylated histone 3 (p-H3) (Fig. 3A) revealed condensed chromatin in ISCs, which is consistent with ISCs being the major mitotic cells in adult *Drosophila* midgut (14,22). *UAS-driven Rab11 RNAi* resulted in a pronounced increase in the number of mitotic enterocytes (Fig. 3B; **see** panels H, I **for quantitation**). Independent experiments using a previously characterized dominant

negative (DN) point mutant *Rab11 S25N* (23) also led to a similar increase in enterocyte mitotic count (**see panel** Fig. 3G **for quantitation**).

Taking advantage of the *Drosophila* midgut genetics model, we examined the impact of Rab11 endosome function on tumorigenesis driven by oncogenic activity via EGFR-activating ($EGFR^{A887T}$) mutation, Ras-activating (Ras^{V12}) mutation, APC loss-of-function (LOF, *APC* RNAi), and Misshapen loss of function (*msn* RNAi) (24). In *Drosophila*, the *Ras V12* mutant is widely used as a cancer model in various fly tissue (25,26). Suppression of *Rab11* expression in combination with the Ras^{V12} mutation (*Rab11RNAi; Ras V12*) led to a significant increase in the number of mitotic cells as compared to Ras^{V12} mutation in Rab11 expressing cells (Fig. 3C, D; **see** panels H, I **for quantitation**). Similarly, *Rab11* inhibition with elevated Wnt signaling, induced by *APC* RNAi (27), led to a significant increase in midgut proliferation as compared to *APC* RNAi in Rab11 expressing cells (Fig. 3E, F; **see** panel I **for quantitation**). Additive effects of loss of *Rab11* with overexpressed Wingless or activated EGFR was not significant (Fig. 3H, I).

To understand the mechanisms contributing to the pro-oncogenic phenotypes initiated by loss of *Rab11*, we performed an unbiased transcriptomic analysis of *Rab11a*-deficient mouse intestines (GEO accession number in process) in parallel with an analysis of *Rab11 RNAi Drosophila* midguts (GEO accession number GSM2435587-GSM2435592). For RNA-seq analysis, intestinal epithelia were collected from $Rab11a^{FL/FL}$*;Villin-CreER* mice two days after tamoxifen administration. Gene set enrichment analysis (GSEA) and heat map analyses uncovered a significant induction of ISC signature genes, for example *Axin2* and *Sox9* upon *Rab11a* deletion ($p<0.001$, N=3 each genotype) (Fig. 4A, B). The increased ISC signature in the transcriptome was reflected by a mild expansion of $Olfm4^{+}$ crypt based columnar cells within 2 days after *Rab11a* disruption (Fig. 4C). The above results demonstrate that disruption of Rab11a expression leads to entry of enterocytes into mitosis with an accompanying promotion of an ISC-like transcriptome as well as a potential linkage to certain oncogenic pathways.

Rab11 activity intersects with Hippo signaling

GSEA analysis of mouse gut 2 days after induced *Rab11a* deletion did not detect a significant enrichment of Yap transcriptional targets ($p=0.13$, Suppl. Fig. 4A). Interestingly by immunocytochemistry, the total and nuclear levels of Yap were significantly elevated in adult *Rab11a*-deficient IECs (Fig. 4D). Nuclear elevation of Yap was observed in crypt cells and some villus epithelial cells, while Paneth cells that are reportedly Yap-negative remain weakly stained in *Rab11a*-deficient IECs (open arrowheads, Fig. 4D). Acute *Rab11a* ablation in adult mouse IECs may not completely remove the protein after 2 days (Suppl. Fig. 4B) and the effect of *Rab11a*-deficiency may also be compensated by *Rab11b*, a Rab11a homolog that is expressed in mouse intestine. Using CRISPR/Cas9 genome editing, a *Rab11b* knockout mouse allele was derived and used this to achieve *Rab11a* and *Rab11b* double knockout (DKO) mice (Suppl. Fig. 4B). Two days after *Rab11a* removal from $Rab11b^{-/-}$ background, a significantly enriched Yap pathway signature was uncovered ($p<0.001$, Fig. 4E). Following tissue specific double knockout (*Rab11a* from $Rab11b^{-/-}$ IECs), there was upregulation of the total Yap and Taz in IECs within 2 days (Fig. 4F). Total

β-catenin levels were not increased, suggesting a selective impact of *Rab11* loss on Yap (Fig. 4F). By day three, all double knockout mice died.

Given the complexity of the mouse gut, enteroid cultures were prepared to determine if changes in Yap protein levels occurred in a cell-autonomous manner. Enteroids from wild type, $Rab11a^{FL/FL}$;*Villin-CreER*, and $Rab11a^{FL/FL}$;$Rab11b^{-/-}$;*Villin-CreER* mice were grown *ex vivo* and *Rab11a* deletion was induced by addition of 4-OHT (Fig. 4G). Quantification of nuclear Yap levels in the eteroids suggest that Rab11 (a & b) protein expression regulates Yap nuclear accumulation in a Rab11 protein dose-dependent fashion (Fig. 4H). In 4-OHT-treated wild type enteroids, Yap was primarily localized to puncta at the apical surface and sub-apical cytoplasm with no detectable nuclear staining (Fig. 4I). Two days after 4-OHT treatment, Yap stained puncta were spread throughout the cytoplasm and nuclear Yap was readily detected in subsets of $Rab11a^{FL/FL}$;*Villin-CreER* cells (Fig. 4J, Suppl. Fig. 4C). In DKO enteroids, Yap location was primarily nuclear (also see arrowheads, Fig. 4K, Suppl. Fig. 4B).

Examination of Yap by immunohistochemistry in AOM-induced tumors in $Rab11a^{\Delta IEC}$ mice revealed uniform nuclear Yap localization in most, if not all, tumor cells (Suppl. Fig. 5A). Tumor cells in 8-week old APC^{Min} mouse intestines (with intact *Rab11a*) had low Yap levels (Fig. 5A, left panel). In contrast, the vast majority of tumors in $Rab11a^{\Delta IEC}$; APC^{Min} mice of the same age showed significantly higher Yap levels ($p<0.001$, Fig. 5A, B, and Suppl. Fig. 5B). Immunoblots confirmed increased Yap levels in both proximal and distal intestines of $Rab11a^{\Delta IEC}$; APC^{Min} mice compared to APC^{Min} littermates (Fig. 5C). A reduced level of phosphorylated Yap (S112) was detected in $Rab11a^{\Delta IEC}$; APC^{Min} samples (Fig. 5C). Yap phosphorylation by LATS regulates Yap cytoplasmic retention and degradation whereas reduced phosphorylation of Yap results in protein stability and elevated nuclear localization (28). Compared to APC^{Min} adenoma, $Rab11a^{\Delta IEC}$; APC^{Min} tumors also exhibited increased levels of Amphiregulin (Areg) (Fig. 5C), an EGF superfamily member reported to be under Yap's regulation (29) and, consistent with Areg upregulation, there were an increased number of tumor cells exhibiting elevated MAPK signaling activity (Fig. 5D). Further, in larger epithelial fields of tumor cells lacking Rab11a there was increased nuclear pStat3 immunostaining (Fig. 5E), likely reflecting an expansion of tumor cell population in response to the elevated inflammatory cytokines, such as IL-6 (11).

To investigate if Rab11A and YAP demonstrated inverse expressional correlation within human colorectal cancers, immunohistochemistry studies were conducted on serial sections of 13 colon tumor samples. The biopsy samples possessed normal and disease tissue ranging from tubulovillous adenoma with high grade dysplasia to stage IV colon cancers. As with mouse tissue, there was an equivalent inverse correlation between Rab11A and YAP expression from normal (high Rab11A, low YAP) versus dysplasia or adenocarcinoma biopsy material (low Rab11A, High YAP) (Fig. 5F, G). Examining the transition from normal epithelia (black dotted lines) to dysplasia (blue dotted lines) to low grade adenoma (red dotted lines) in stage I cancer tissue revealed an immediately reversed expression pattern of the two proteins (Fig. 5F).

Loss of *Drosophila* Hippo and Misshapen, two upstream Sterile 20/germinal center kinases that suppress the growth-promoting transcriptional co-activator Yki to regulate growth factor production, has been shown to increase ISC proliferation (30,31). Given the discovered *Drosophila* and mouse linkage of Yki/Yap activation in *Rab11*-deficient guts (Fig. 4E, 6A), we examined the genetic interaction between Rab11 and Hippo-Yki pathway in *Drosophila* midgut. Two of the most significantly elevated targets in *Rab11* RNAi fly midgut were *upd3* (homolog of mammalian IL-6) and *ImpL2* (homolog of mammalian IGFBP7) (Fig. 6B, C, D). IL-6 is a pro-inflammatory cytokine shown to promote colon cancer progression (32), while ImpL2 secreted from cancer tissues are shown to inhibit whole animal metabolism in various *Drosophila* cancer models involving Yki or Scribble (33). Loss of *Rab11* synergized with Ras^{V12} mutation, leading to a near 780-fold and 70-fold induction of *upd3/IL-6* and *ImpL2*, respectively (Fig. 6C). Furthermore, inclusion of a loss-of-function mutant allele of *upd3* (17) as homozygotes led to a significant suppression of mitotic counts in *Rab11* RNAi midgut (Fig. 6E). These results functionally confirmed that *upd3* played an important role in promoting elevated proliferation and tissue growth observed in *Rab11*-deficient gut.

Since Yki activation of *upd3* expression is normally restricted by the upstream Ste20 kinases Hippo and Misshapen (34), we tested whether expression of constitutively active Yki was sufficient to induce phenotypes and transcriptomic changes observed in *Rab11 RNAi; Ras^{V12}* mice. Using the *Myo1A-Gal4* driver, a constitutively active Yki construct (Yki^{Act}), containing three mutated phosphorylation sites that eliminated regulation by upstream kinases (18), was expressed in fly midgut enterocytes. The experimental design mimics in fly the reduced pYAP observed in mouse gut (Fig. 5C). Overexpressing Yki^{Act} led to highly increased mitotic count (Fig. 6F) and elevated *upd3* and *ImpL2* transcription (Fig. 6G). To determine whether suppressing Yki could alleviate *Rab11* RNAi midgut phenotypes, experiments were conducted combining *Yki* RNAi and *Rab11* RNAi. Double RNAi led to partial suppression of *Rab11* RNAi midgut phenotypes (Fig. 6H–O). Most notably, *Yki* RNAi suppressed the dysplastic multi-layered epithelial structure induced by *Rab11* RNAi and the midgut now possessed a more typical monolayer structure (Fig. 6L–O). These genetic experiments collectively suggest that elevated Yki activity in fly accounts for some phenotypes seen in *Rab11*-deficient gut and suppressing Yki alleviates the dysplastic phenotype.

Immunoblot analysis across a panel of 7 human colon cancer cell lines showed that Caco2 and LIM2551 expressed the highest levels of Rab11A and relatively lowest levels of YAP/TAZ. SW480, LIM1215, and LIM2550 cells had low Rab11A levels and exhibited relatively higher YAP/TAZ levels (Fig. 7A). Following this lead, three stable *RAB11A*-knockdown (KD) cell lines were prepared using Caco2, SW480, and LIM2551 and lentiviral siRNA infection (Fig. 7B). These cell lines have distinct oncogenic mutations in *APC* and *K-RAS* (35). Rab11A-KD Caco2 and SW480 cells showed increased total YAP/TAZ (Fig. 7B) and all three lines have reduced pYAP at S127 (Fig. 7B, C). Phosphorylation of human YAP at S127 serves as a cytoplasmic retention signal (36) and reduced levels of S127 phosphorylation resulted in elevated levels of YAP in biochemically isolated nuclei (Fig. 7D and 7E). Rab11A-KD Caco2 and LIM2551 cells also exhibited decreased phosphorylation of YAP at serine 397 (Fig. 7F) that would result in decreased proteasome-mediated YAP degradation (36). Increased nuclear YAP was correlated with elevated levels of AREG and

IL-6 (Fig. 7F, G); SW480 cells did not express detectable levels of AREG. Using a TEAD reporter (37), we detected significantly elevated canonical YAP activity in *RAB11A*-KD SW480 cells (Suppl. Fig. 6A). Chromatin immunoprecipitation (ChIP) for YAP1 demonstrated that in both Caco2 and SW480 cells, *RAB11A*-deficiency increased YAP1 chromatin association with its targets: LATS2, TEAD1, and CCND1 (Suppl. Fig. 6B, C). All of the cumulative data presented in the above section indicate that elevated YAP activity can cell-autonomously regulate the expression of YAP targets.

Phosphorylation of YAP at S127 in humans or S112 in mice is mediated by the LATS1 kinase that itself is activated by phosphorylation through the upstream Hippo kinase cascade. *Rab11A*-KD Caco2 cells showed no significant difference in the total level of Hippo complex components that control YAP activity including MST1, LATS1, MOB1, SAV1, or exportin-1 or α-catenin as compared to controls (Fig. 7H) (38). Phosphorylation of LATS1 is reported to occur following trafficking to the apical junctions to suppress YAP (39). Interestingly, there were observable reductions in the levels of phosphorylated LATS1 at T1079, S909, or S872 in *Rab11A*-KD cells (Fig. 7I). Additionally, by immunofluorescence staining, there was readily detectable localization of YAP to cell-cell junctions (arrows, Fig. 7J). In Rab11A-KD cells YAP was noticeably enriched in nuclei (Fig. 7K) while junctional localization was effectively lost in these cells (Fig. 7L). These data collectively suggest that Rab11a may likely play a key role in junctional delivery and/or assembly of key Hippo kinase-dependent molecules that are essential for regulation of YAP activity.

DISCUSSION

Taking advantage of several genetic models, this report demonstrated that Rab11 protein has the capability of restraining uncontrolled cell growth and progression of colon cancers. The results suggest that perturbation of recycling endosome traffic, a hallmark function in epithelia, can influence differentiated epithelial cell status by unbalancing signaling pathways leading to reversion into a progenitor-like, proliferative cell state. Additionally, altered expression and localization of RAB11A in colon cancer tumors suggest that altered recycling endosomal functionality may participate in accelerating cancer progression.

Our results support the view that perturbation of recycling endosome assembly/trafficking is sufficient to induce early onset epithelial dysplasia leading to an oncogenic cue for uncontrolled growth. Loss of mouse Rab25, a member of Rab11 superfamily, was shown previously to increase intestinal tumor burden in mice carrying APC mutation. *Rab25*-deficient mouse intestinal tumor cells also exhibited reduced integrin expression, thereby enhancing invasive behavior in a Smad3 haploid insufficiency background (40). Our genetic experiments on Rab11 in fly and mouse gut showed that perturbation of this small GTPase robustly synergizes with various oncogenic driver mutations, including *APC* loss-of-function and Ras^{V12} to promote not only the production of pro-growth inflammatory cytokines, e.g., upd3/IL-6 and Areg, but also the expansion of a tumorigenic stem cell pool. Rescue experiments suppressing Yap/Yki, or its target IL6/Upd3, in *Rab11*-deficient gut reduced the dysplastic and hyperplastic growth, supporting a conclusion that the observed rapid tumor expansion was in part due to the elevated inflammatory proteins produced in the *Rab11*-deficient tissue microenvironment.

Further, unbiased meta data analysis revealed reduced RAB11A mRNA level in the majority of documented colon cancers. In our analysis, most of the colon cancers showed altered Rab11a apical localization and a strong inverse correlation between Rab11a expression and total YAP cellular levels. Reduced and altered apical Rab11a localization has been reported in human congenital enteropathy (41). RAB11 was also reported to be upregulated in several non-intestinal tumors including non-small cell lung carcinoma (42), skin tumors (43), and pancreatic cancers (44). Also, ~9% of colon cancers showed elevated RAB11A level when compared to normal colonic epithelia however, survival analysis of colon cancer patients using the TCGA database demonstrated that only those patients with reduced RAB11A displayed significantly poorer rates of survival. Thus, the RAB11 endosomal compartment may have context- or cell-type-dependent functions in tumorigenesis. Caution should be taken for any proposed therapeutic targeting of this molecular machinery (45).

Rab11 endosomes traffic a diverse spectrum of membrane and secretory proteins, and our transcriptomic study discovered a previously unrecognized link to important growth pathways. In intestinal epithelia, across various species, Rab11 perturbation appeared to intersect with the Hippo pathway. Experiments with mouse enteroids support a cell-autonomous effect of loss-of-Rab11 on Yap nuclear translocation. In prior work, we reported that induced deletion of *Rab11a* from intestinal epithelia led to rapid aberrant formation of apical membrane structures, such as the microvilli, at the basolateral cellular domains (12,13,46) and now RNA-seq analysis detected genome-wide activation of stem cell transcriptomic program. In addition, *Rab11a* removal from *Rab11b−/−* IECs led to immediate alteration of the YAP pathway and death of the animals within 3 days. Although this lethality phenotype was reminiscent of transgenic mice that died after a week of induced overexpression of YAP(S127A) mutant (47), the loss-of-function of Rab11a/b appeared to have a more robust phenotype implicating a broad molecular impact that warrants future study. Our current work provides substantial *in vivo* evidence that perturbing Rab11 endosome functionality can rapidly and cell-autonomously alter Hippo signaling and accelerate colon cancer development (48–52). At this point, we speculate that RAB11 endosomes transport key Hippo pathway components to sites of YAP regulation or endosomal sorting may provide a scaffolding platform for Hippo complex assembly and YAP suppression.

Supplementary Material

Refer to Web version on PubMed Central for supplementary material.

ACKNOWLEDGEMENT:

We thank the Facility of Genome Editing of Rutgers Cancer Institute of New Jersey (P30CA072720) for developing Rab11b-null mice and the Perceval HPC cluster (NIH grant # 1S10OD012346-01A1) for computational analysis. Work was supported by: NIH (CA178599, DK102934, AT010243, DK119198), ACS Scholar Award (RSG-15-060-01-TBE), NSF/BIO/IDBR (1353890), and a Rutgers IMRT award to N.G.; NIH/NCI R01CA190558 to M.P.V.; R01 DK70856 to J.R.G; a NSF Grant (IOS-1456673, IOS-1754783) to R.P.F.; a CCFA career development award (406794) to S.Y.; R01DK102934-S1 to I.J.; NIH grants (GM107457, DK083450), UMass DERC (DK32520), UMass Center for Clinical and Translational Science (UL1TR000161), Guangdong Innovative Research Team Program (No. 201001Y0104789252) and the Science and Technology Program of Guangzhou (No. 201704030044) to Y.T.I.; NJCCR fellowships (DFHS16PPC038, DHFS16PPC036, DFHS17PPC036, DCHS19PPC038) to S.G., K.T., S.B., J.F., respectively; and NIH R25 IMSD Grant (2R25GM096161-08) to J.F.

References

1. Tong K, Pellon-Cardenas O, Sirihorachai VR, Warder BN, Kothari OA, Perekatt AO, et al. Degree of Tissue Differentiation Dictates Susceptibility to BRAF-Driven Colorectal Cancer. Cell Rep 2017;21:3833–45 [PubMed: 29281831]
2. Lieberman DA, Rex DK, Winawer SJ, Giardiello FM, Johnson DA, Levin TR. Guidelines for colonoscopy surveillance after screening and polypectomy: a consensus update by the US Multi-Society Task Force on Colorectal Cancer. Gastroenterology 2012;143:844–57 [PubMed: 22763141]
3. Hanahan D, Weinberg RA. Hallmarks of cancer: the next generation. Cell 2011;144:646–74 [PubMed: 21376230]
4. Goldenring JR. A central role for vesicle trafficking in epithelial neoplasia: intracellular highways to carcinogenesis. Nat Rev Cancer 2013;13:813–20 [PubMed: 24108097]
5. Goldenring JR. Recycling endosomes. Curr Opin Cell Biol 2015;35:117–22 [PubMed: 26022676]
6. Sasikumar S, Roy JK. Developmental expression of Rab11, a small GTP-binding protein in Drosophila epithelia. Genesis 2009;47:32–9 [PubMed: 19039786]
7. Bogard N, Lan L, Xu J, Cohen RS. Rab11 maintains connections between germline stem cells and niche cells in the Drosophila ovary. Development 2007;134:3413–8 [PubMed: 17715175]
8. Xu J, Lan L, Bogard N, Mattione C, Cohen RS. Rab11 is required for epithelial cell viability, terminal differentiation, and suppression of tumor-like growth in the Drosophila egg chamber. PLoS ONE 2011;6:e20180 [PubMed: 21629779]
9. Gao N, Kaestner KH. Cdx2 regulates endo-lysosomal function and epithelial cell polarity. Genes Dev 2010;24:1295–305 [PubMed: 20551175]
10. Yu S, Yehia G, Wang J, Stypulkowski E, Sakamori R, Jiang P, et al. Global ablation of the mouse Rab11a gene impairs early embryogenesis and matrix metalloproteinase secretion. J Biol Chem 2014;289:32030–43 [PubMed: 25271168]
11. Yu S, Nie Y, Knowles B, Sakamori R, Stypulkowski E, Patel C, et al. TLR sorting by Rab11 endosomes maintains intestinal epithelial-microbial homeostasis. EMBO J 2014;33:1882–95 [PubMed: 25063677]
12. Knowles BC, Weis VG, Yu S, Roland JT, Williams JA, Alvarado GS, et al. Rab11a regulates Syntaxin 3 localization and microvillus assembly in enterocytes. J Cell Sci 2015
13. Feng Q, Bonder EM, Engevik AC, Zhang L, Tyska MJ, Goldenring JR, et al. Disruption of Rab8a and Rab11a causes formation of basolateral microvilli in neonatal enteropathy. J Cell Sci 2017;130:2491–505 [PubMed: 28596241]
14. Micchelli CA, Perrimon N. Evidence that stem cells reside in the adult Drosophila midgut epithelium. Nature 2006;439:475–9 [PubMed: 16340959]
15. Amcheslavsky A, Jiang J, Ip YT. Tissue damage-induced intestinal stem cell division in Drosophila. Cell Stem Cell 2009;4:49–61 [PubMed: 19128792]
16. Jiang H, Patel PH, Kohlmaier A, Grenley MO, McEwen DG, Edgar BA. Cytokine/Jak/Stat signaling mediates regeneration and homeostasis in the Drosophila midgut. Cell 2009;137:1343–55 [PubMed: 19563763]
17. Zhou F, Rasmussen A, Lee S, Agaisse H. The UPD3 cytokine couples environmental challenge and intestinal stem cell division through modulation of JAK/STAT signaling in the stem cell microenvironment. Dev Biol 2013;373:383–93 [PubMed: 23110761]
18. Kwon Y, Song W, Droujinine IA, Hu Y, Asara JM, Perrimon N. Systemic organ wasting induced by localized expression of the secreted insulin/IGF antagonist ImpL2. Dev Cell 2015;33:36–46 [PubMed: 25850671]
19. Suzuki R, Kohno H, Sugie S, Nakagama H, Tanaka T. Strain differences in the susceptibility to azoxymethane and dextran sodium sulfate-induced colon carcinogenesis in mice. Carcinogenesis 2006;27:162–9 [PubMed: 16081511]
20. Cheung C, Loy S, Li GX, Liu AB, Yang CS. Rapid induction of colon carcinogenesis in CYP1A-humanized mice by 2-amino-1-methyl-6-phenylimidazo[4,5-b]pyridine and dextran sodium sulfate. Carcinogenesis 2011;32:233–9 [PubMed: 21081470]

21. Perrimon N, Lanjuin A, Arnold C, Noll E. Zygotic lethal mutations with maternal effect phenotypes in Drosophila melanogaster. II. Loci on the second and third chromosomes identified by P-element-induced mutations. Genetics 1996;144:1681–92 [PubMed: 8978055]
22. Ohlstein B, Spradling A. The adult Drosophila posterior midgut is maintained by pluripotent stem cells. Nature 2006;439:470–4 [PubMed: 16340960]
23. Breda C, Nugent ML, Estranero JG, Kyriacou CP, Outeiro TF, Steinert JR, et al. Rab11 modulates alpha-synuclein-mediated defects in synaptic transmission and behaviour. Hum Mol Genet 2015;24:1077–91 [PubMed: 25305083]
24. Yan H, Jahanshahi M, Horvath EA, Liu HY, Pfleger CM. Rabex-5 ubiquitin ligase activity restricts Ras signaling to establish pathway homeostasis in Drosophila. Curr Biol 2010;20:1378–82 [PubMed: 20655224]
25. Lee T, Feig L, Montell DJ. Two distinct roles for Ras in a developmentally regulated cell migration. Development 1996;122:409–18 [PubMed: 8625792]
26. Jiang H, Grenley MO, Bravo MJ, Blumhagen RZ, Edgar BA. EGFR/Ras/MAPK signaling mediates adult midgut epithelial homeostasis and regeneration in Drosophila. Cell Stem Cell 2011;8:84–95 [PubMed: 21167805]
27. Lee WC, Beebe K, Sudmeier L, Micchelli CA. Adenomatous polyposis coli regulates Drosophila intestinal stem cell proliferation. Development 2009;136:2255–64 [PubMed: 19502486]
28. Zhao B, Wei X, Li W, Udan RS, Yang Q, Kim J, et al. Inactivation of YAP oncoprotein by the Hippo pathway is involved in cell contact inhibition and tissue growth control. Genes & Development 2007;21:2747–61 [PubMed: 17974916]
29. Han S-x, Bai E, Jin G-h, He C-c, Guo X-j, Wang L-j, et al. Expression and Clinical Significance of YAP, TAZ, and AREG in Hepatocellular Carcinoma. Journal of Immunology Research 2014;2014:261365 [PubMed: 24860833]
30. Staley BK, Irvine KD. Warts and Yorkie mediate intestinal regeneration by influencing stem cell proliferation. Curr Biol 2010;20:1580–7 [PubMed: 20727758]
31. Li Q, Li S, Mana-Capelli S, Roth Flach RJ, Danai LV, Amcheslavsky A, et al. The conserved misshapen-warts-Yorkie pathway acts in enteroblasts to regulate intestinal stem cells in Drosophila. Dev Cell 2014;31:291–304 [PubMed: 25453828]
32. Waldner MJ, Foersch S, Neurath MF. Interleukin-6 - A Key Regulator of Colorectal Cancer Development. International Journal of Biological Sciences 2012;8:1248–53 [PubMed: 23136553]
33. Figueroa-Clarevega A, Bilder D. Malignant Drosophila tumors interrupt insulin signaling to induce cachexia-like wasting. Dev Cell 2015;33:47–55 [PubMed: 25850672]
34. Ren F, Wang B, Yue T, Yun EY, Ip YT, Jiang J. Hippo signaling regulates Drosophila intestine stem cell proliferation through multiple pathways. Proc Natl Acad Sci U S A 2010;107:21064–9 [PubMed: 21078993]
35. Rhodes DR, Kalyana-Sundaram S, Mahavisno V, Varambally R, Yu J, Briggs BB, et al. Oncomine 3.0: genes, pathways, and networks in a collection of 18,000 cancer gene expression profiles. Neoplasia (New York, NY) 2007;9:166–80
36. Zhao B, Li L, Tumaneng K, Wang C-Y, Guan K-L. A coordinated phosphorylation by Lats and CK1 regulates YAP stability through SCF(β-TRCP). Genes & Development 2010;24:72–85 [PubMed: 20048001]
37. Dupont S, Morsut L, Aragona M, Enzo E, Giulitti S, Cordenonsi M, et al. Role of YAP/TAZ in mechanotransduction. Nature 2011;474:179–83 [PubMed: 21654799]
38. Schlegelmilch K, Mohseni M, Kirak O, Pruszak J, Rodriguez JR, Zhou D, et al. Yap1 acts downstream of α-catenin to control epidermal proliferation. Cell 2011;144:782–95 [PubMed: 21376238]
39. Szymaniak Aleksander D, Mahoney John E, Cardoso Wellington V, Varelas X. Crumbs3-Mediated Polarity Directs Airway Epithelial Cell Fate through the Hippo Pathway Effector Yap. Developmental Cell 2015;34:283–96 [PubMed: 26235047]
40. Nam KT, Lee HJ, Smith JJ, Lapierre LA, Kamath VP, Chen X, et al. Loss of Rab25 promotes the development of intestinal neoplasia in mice and is associated with human colorectal adenocarcinomas. Journal of Clinical Investigation 2010;120:840–9 [PubMed: 20197623]

41. Talmon G, Holzapfel M, DiMaio DJ, Muirhead D. Rab11 is a useful tool for the diagnosis of microvillous inclusion disease. International journal of surgical pathology 2012;20:252–6 [PubMed: 22169970]
42. Dong Q, Fu L, Zhao Y, Du Y, Li Q, Qiu X, et al. Rab11a promotes proliferation and invasion through regulation of YAP in non-small cell lung cancer. Oncotarget 2017;8:27800–11 [PubMed: 28468127]
43. Gebhardt C, Breitenbach U, Richter KH, Fürstenberger G, Mauch C, Angel P, et al. c-Fos-Dependent Induction of the Small Ras-Related GTPase Rab11a in Skin Carcinogenesis. The American Journal of Pathology 2005;167:243–53 [PubMed: 15972968]
44. Yu L, Li X, Li H, Chen H, Liu H. Rab11a sustains GSK3beta/Wnt/beta-catenin signaling to enhance cancer progression in pancreatic cancer. Tumour biology : the journal of the International Society for Oncodevelopmental Biology and Medicine 2016;37:13821–9 [PubMed: 27481517]
45. Qin X, Wang J, Wang X, Liu F, Jiang B, Zhang Y. Targeting Rabs as a novel therapeutic strategy for cancer therapy. Drug discovery today 2017;22:1139–47 [PubMed: 28390930]
46. Zhang X, Gao N. RAB and RHO GTPases regulate intestinal crypt cell homeostasis and enterocyte function. Small GTPases 2016;7:59–64 [PubMed: 27142493]
47. Barry ER, Morikawa T, Butler BL, Shrestha K, de la Rosa R, Yan KS, et al. Restriction of intestinal stem cell expansion and the regenerative response by YAP. Nature 2013;493:106–10 [PubMed: 23178811]
48. Ling HH, Kuo CC, Lin BX, Huang YH, Lin CW. Elevation of YAP promotes the epithelial-mesenchymal transition and tumor aggressiveness in colorectal cancer. Exp Cell Res 2017;350:218–25 [PubMed: 27914787]
49. Sun Z-Q, Shi K, Zhou Q-B, Zeng X-Y, Liu J, Yang S-X, et al. MiR-590-3p promotes proliferation and metastasis of colorectal cancer via Hippo pathway. Oncotarget 2017;8:58061–71 [PubMed: 28938537]
50. Wang L, Shi S, Guo Z, Zhang X, Han S, Yang A, et al. Overexpression of YAP and TAZ is an independent predictor of prognosis in colorectal cancer and related to the proliferation and metastasis of colon cancer cells. PLoS One 2013;8:e65539 [PubMed: 23762387]
51. Zhou D, Zhang Y, Wu H, Barry E, Yin Y, Lawrence E, et al. Mst1 and Mst2 protein kinases restrain intestinal stem cell proliferation and colonic tumorigenesis by inhibition of Yes-associated protein (Yap) overabundance. Proc Natl Acad Sci U S A 2011;108:E1312–20 [PubMed: 22042863]
52. Camargo FD, Gokhale S, Johnnidis JB, Fu D, Bell GW, Jaenisch R, et al. YAP1 increases organ size and expands undifferentiated progenitor cells. Curr Biol 2007;17:2054–60 [PubMed: 17980593]

Statement of significance:

Recycling endosome traffic in mature epithelia constitutes a novel tumor suppressing mechanism.

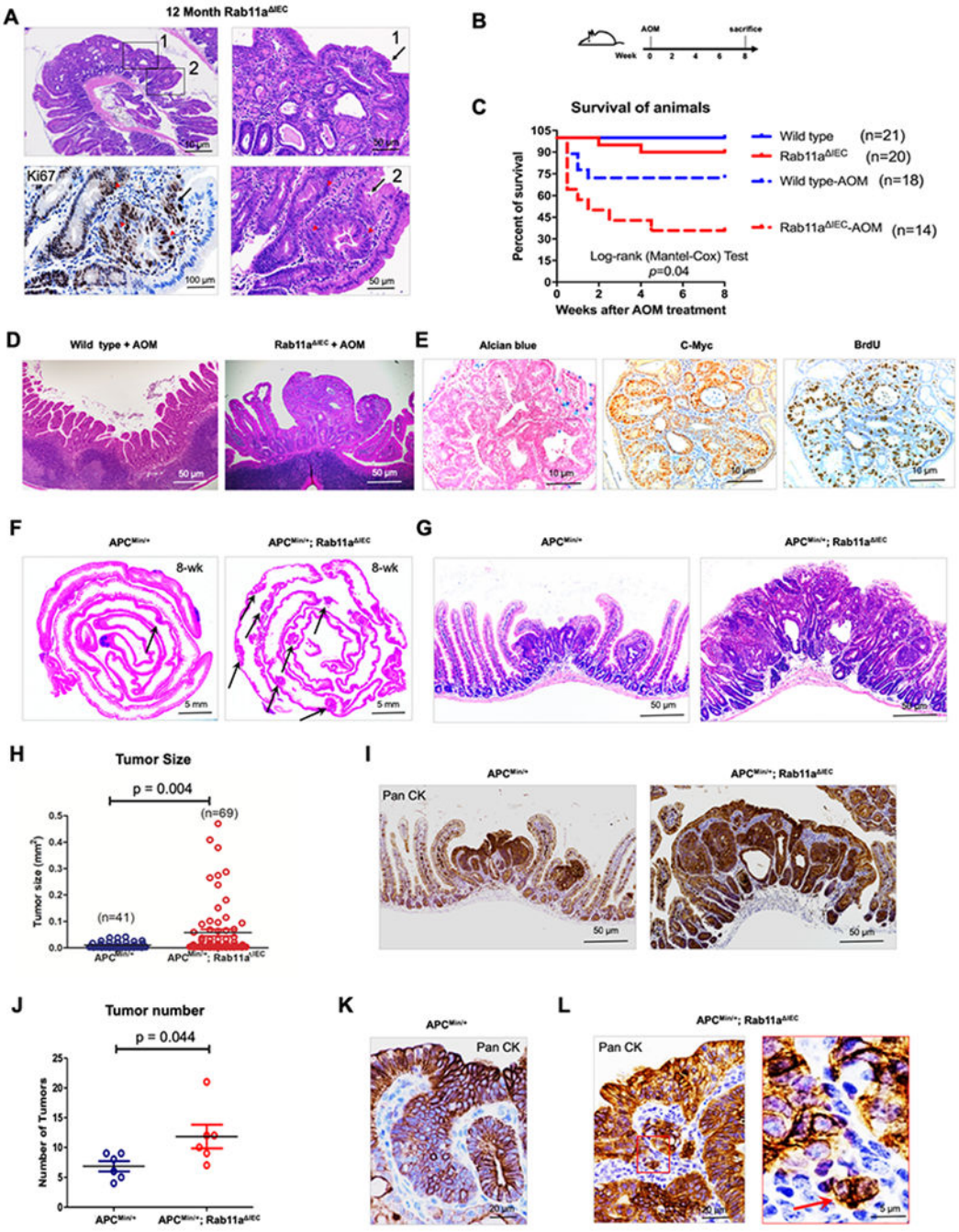

Figure 1. Rab11a deficiency accelerates tumorigenesis.

(A) Analysis of dysplasia and adenoma year-old Rab11a$^{\Delta IEC}$ mice. Boxes indicate area of tubular adenomas (magnified in 1) and high-grade dysplasia (magnified in 2). Ki67 staining (arrows) identifies proliferative adenoma cells.

(B) Experimental scheme for AOM treatment on day 0 followed by tissue harvest at 8 weeks.

(C) AOM-treated Rab11a$^{\Delta IEC}$ mice show significantly increased mortality compared to WT mice (combined data from 6 independent experiments).

(D) Representative histological image of AOM-treated mouse distal intestine showing tubular adenomas in Rab11a$^{\Delta IEC}$ animals (right panel).
(E) Adenomas of AOM-treated Rab11a$^{\Delta IEC}$ mice show loss of goblet cells, c-Myc staining, and enhanced proliferation.
(F-G) Eight-week old APC^{Min}; Rab11a$^{\Delta IEC}$ mice show increased tumor size compared to littermate APC^{Min} mice. Note the horizontally expanded tumor mass and complex tumor architecture in APC^{Min}; Rab11a$^{\Delta IEC}$ mice in G.
(H) Individual tumors sizes from APC^{Min} or APC^{Min}; Rab11a$^{\Delta IEC}$ mouse intestines were measured using histological sections (n=3 for each genotype).
(I) Immunohistochemistry for pan-cytokeratin highlights increased tumor size with high-grade dysplasia.
(J) APC^{Min}; Rab11a$^{\Delta IEC}$ mice showed increased tumor numbers along the full-length intestinal tract (n=3 for each genotype).
(K, L) Immunohistochemistry for pan-cytokeratin shows infiltrating cells with intramucosal invasive feature (arrow) in APC^{Min}; Rab11a$^{\Delta IEC}$ mice.

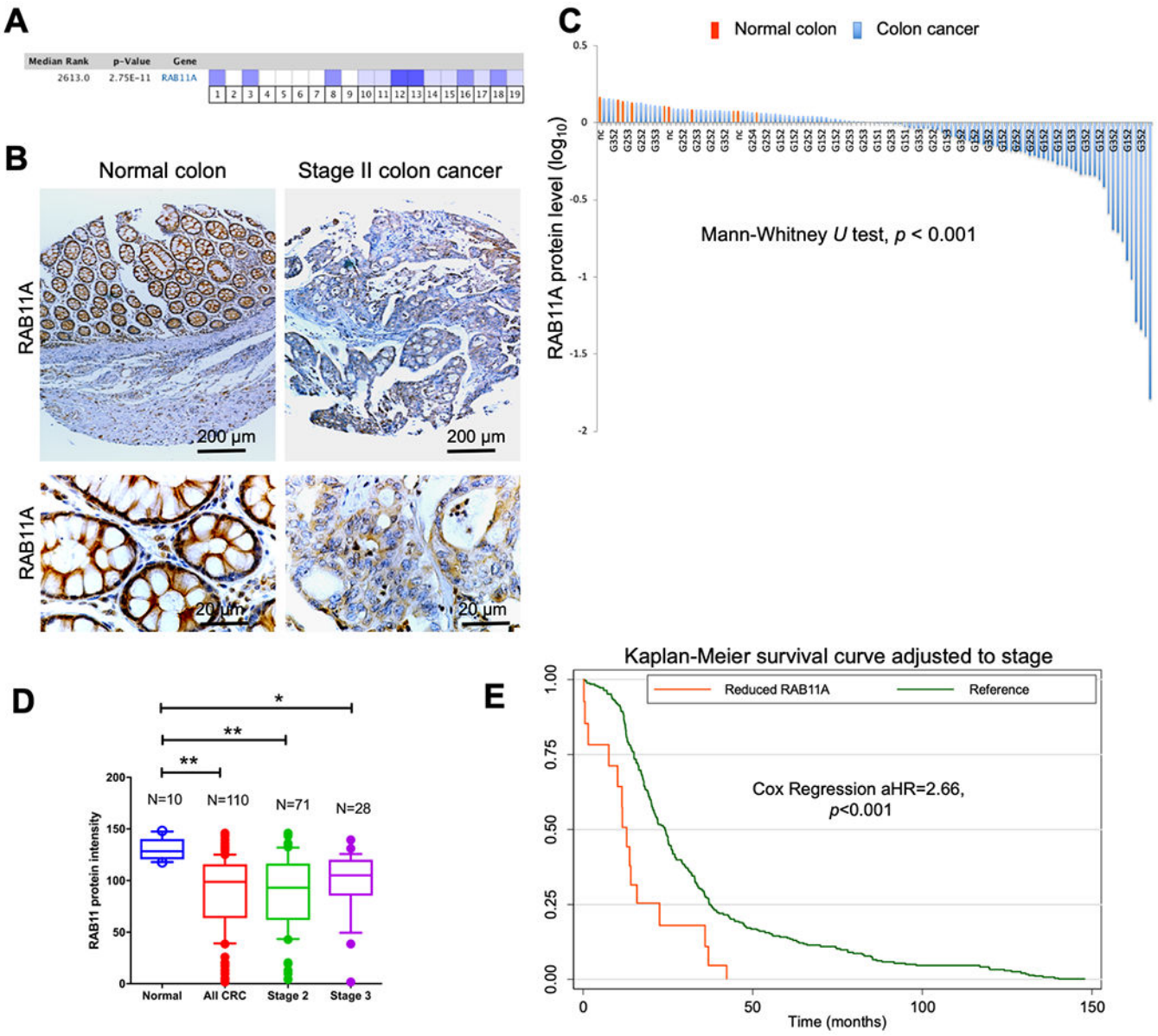

Figure 2. Expression and apical localization of RAB11A in human colon cancers.

(A) ONCOMINE across 19 database shows significant RAB11A mRNA reduction in colon cancers.

(B) Immunohistochemistry for Rab11a using a colon cancer tissue microarray (110 cancers and 10 normal) displayed reduced Rab11a protein in cancer tissue. Representative normal and stage II adenocarcinoma are shown.

(C) Average Rab11a levels of individual samples are ranked and the vast majority of colon cancers show reduced Rab11a levels ($p<0.001$) while only 10 colon cancers show increased Rab11a compared to average values for normal tissue. Normal tissue in red and cancer tissue in blue.

(D) Rab11a levels are significantly reduced in stage II and II colon cancers.

(E) Kaplan-Meier survival analysis of colon cancer patients in TCGA shows poorer survival of those with the lowest Rab11a level (the lower 5 percentile, n=16) than the reference (n=298).

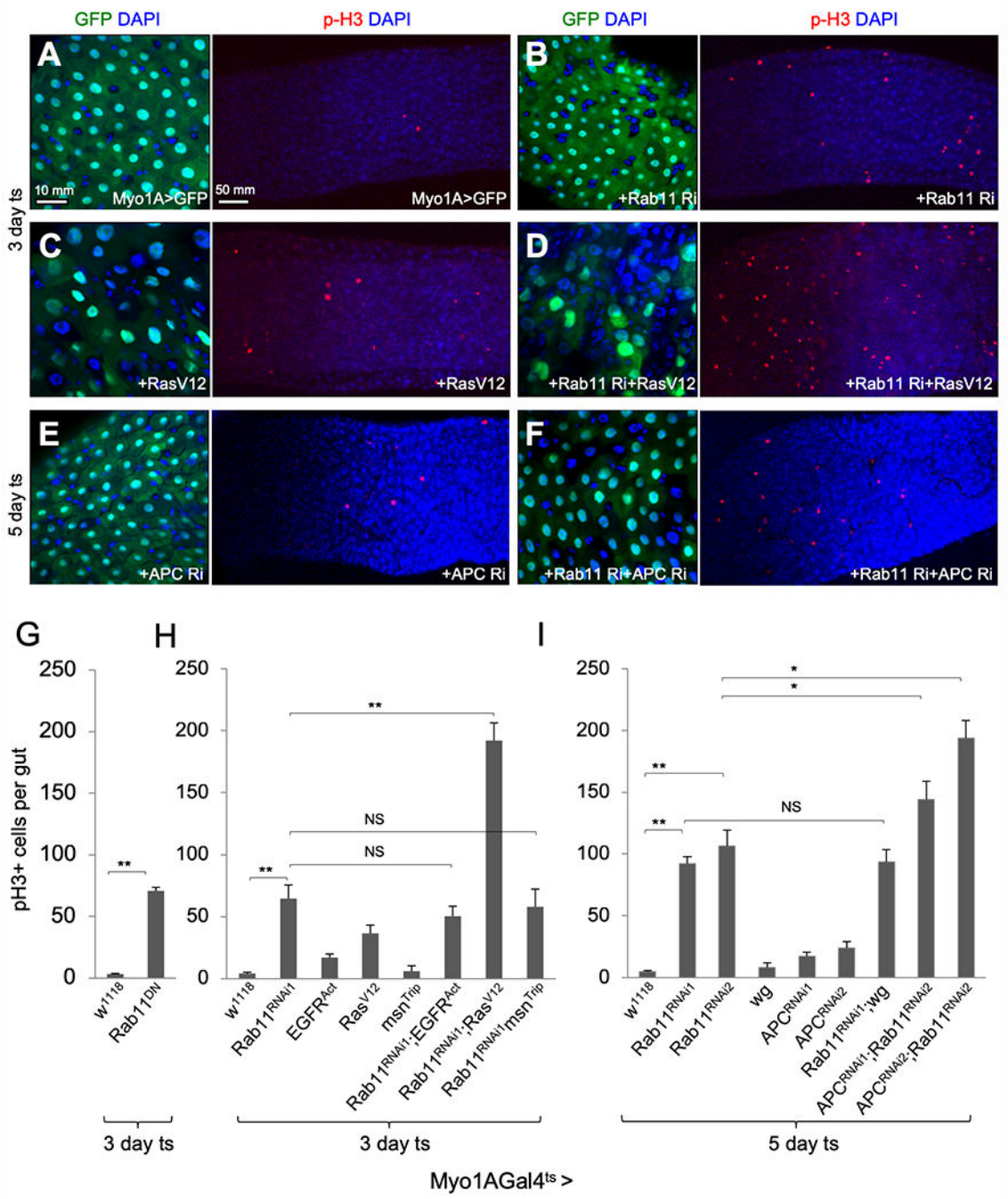

Figure 3. Loss Rab11 function links to oncogenic pathways in Drosophila midgut proliferation.

Adult flies containing the Myo1AGal4ts-UAS-GFP driver/marker transgenes were aged for 5-7 days at ~22°C, shifted to 29°C for 3 days to allow the inactivation of the Gal80ts repressor and drive transgenic expression.

(A) Confocal micrograph of posterior midgut surface showing merged DAPI and Myo1A driven GFP expression in both cytoplasm and nucleus of enterocytes (left panel). Small cell clusters lacking a GFP signal are ISC/precursor cell nests containing single or double nuclei.

The right panel is a lower magnification of the midgut of the same genotype stained for p-H3 to identify mitotic cells. DAPI staining for DNA in blue.

(B) Confocal images of posterior midgut expressing UAS-Rab11 RNAi driven by the Myo1AGal4 line. (Left panel). Labeled nest cells (left panel) have a greater frequency of detecting multinucleate ISCs indicating increased mitotic activity. Increased mitotic activity is identified by increased p-H3 staining (right panel).

(C) Confocal images of posterior midgut containing the UAS-Ras^{V12} cDNA detected a slight increase in mitotic nest cells (left and right panels).

(D) Combining both UAS-Rab11 RNAi and UAS-Ras^{V12} cDNA constructs resulted in marked increase in p-H3 staining over flies modified with single constructs.

(E) Confocal images of midgut expressing UAS-APC RNAi after 5 days at 29°C.

(F) Confocal image of midgut expressing both UAS-Rab11 RNAi and UAS-APC RNAi constructs.

(G) Midguts from control flies or flies expressing a Rab11 dominant negative (DN) construct were stained for p-H3 and stained nuclei of >10 midguts from 3 individual experiments were counted for each sample. The average pH3+ nuclear count was over 50 times greater in DN flies. Error bar = SEM; ** = p value<0.01.

(H) Quantitation of p-H3 stained nuclei as described above was conducted for flies with constructs for Rab11 RNAi, activated EGFR, Ras^{V12}, msn RNAi, or construct combinations as indicated.

(I) Mitotic cell counts of midguts from flies expressing constructs for Rab11 RNAi, Wingless (wg) cDNA, a second APC RNAi constructs, or combinations as indicated. The temperature shift was for 5 days to boost the expression response.

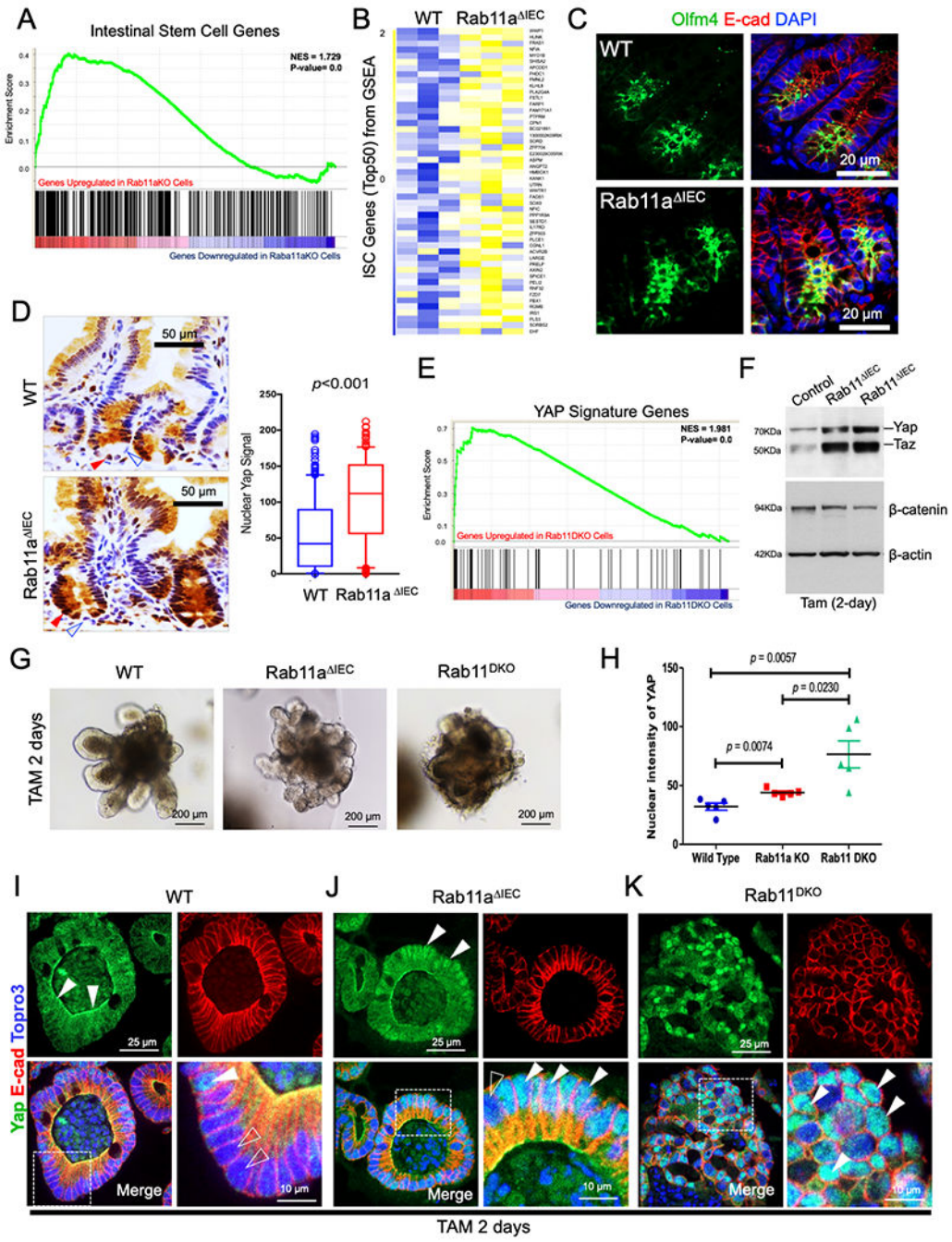

Figure 4. Rab11 ablation activates a stem cell signature and Yap signaling.

(A) GSEA analysis identified enriched stem cell gene signature within 2 days after Rab11a deletion from mouse IECs.

(B) Heat map for top 50 stem cell genes upregulated upon Rab11a deletion.

(C) Immunolocalization of Olfm4 (green) labeled crypt stem cells in WT and epithelial cells 2-days after tamoxifen injection to delete Rab11a.

(D) Rab11a deletion by Vil-Cre increased total Yap levels and Yap+ nuclei (red arrowheads) in both crypt and villus compartments. Paneth cells remained Yap negative (open arrowheads).
(E) Yap signature genes are upregulated after induced Rab11 deletion.
(F) Total Yap/Taz levels are increased 2 days post Rab11 deletion. Total β-catenin levels were not increased in the same tissues.
(G) Representative images of enteroids cultured from wild type, $Rab11^{FL/FL}$; Vil-CreER, and $Rab11^{FL/FL}$; Vil-CreER; $Rab11b^{-/-}$ mice 2 days after 4-OHT treatment.
(H) Nuclear Yap levels increased in Rab11a-deficient and DKO enteroid cells.
(I-K) Immunofluorescent staining of sectioned enteroids for Yap (green) and E-cad (red). In higher magnification images (lower right panels in I, J, K), solid arrowheads point to nuclear Yap, while empty arrowhead indicates Yap-negative nucleus.

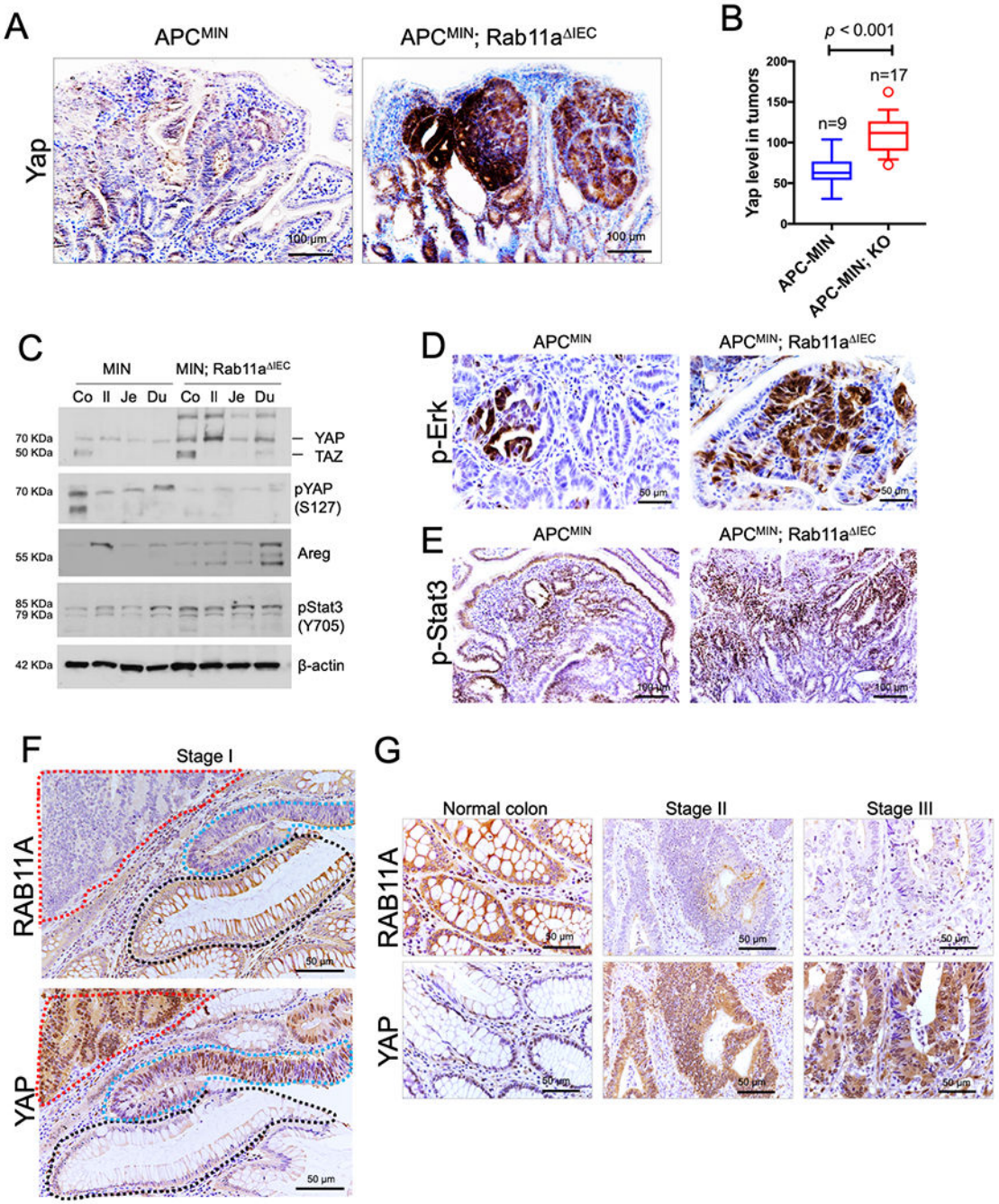

Figure 5. Rab11a-deficient tumor cells have elevated Yap, MAPK, and Stat3 signaling.

(A and B) Immunohistochemistry and quantitative analysis revealed elevated total Yap in Rab11a-deficient APC^{Min} tumors.

(C) Western blots of various mouse gut segments (colon (Co), ileum (Il), jejunum (Je), and duodenum (Du) show increased Yap/Taz, Areg, pStat3-Tyr705, and decreased pYap-S112 (note: probed with anti-human pYap-S127 antibodies) levels in $Rab11^{FL/FL}$; Vil-Cre; APC^{Min} mice as compared to APC^{Min} littermates.

(D-E) Immunohistochemistry showed increased Rab11a-deficient tumor cells have high levels of p-Erk and pStat3.
(F) Stage I CRC tumor showed inverse RAB11A and YAP expression in normal epithelia (black dotted line) adenoma (blue dotted line), and invasive carcinoma (red dotted line).
(G) Immunohistochemistry on adjacent human colon cancer sections showed similar inverse correlation between RAB11A and YAP expression.

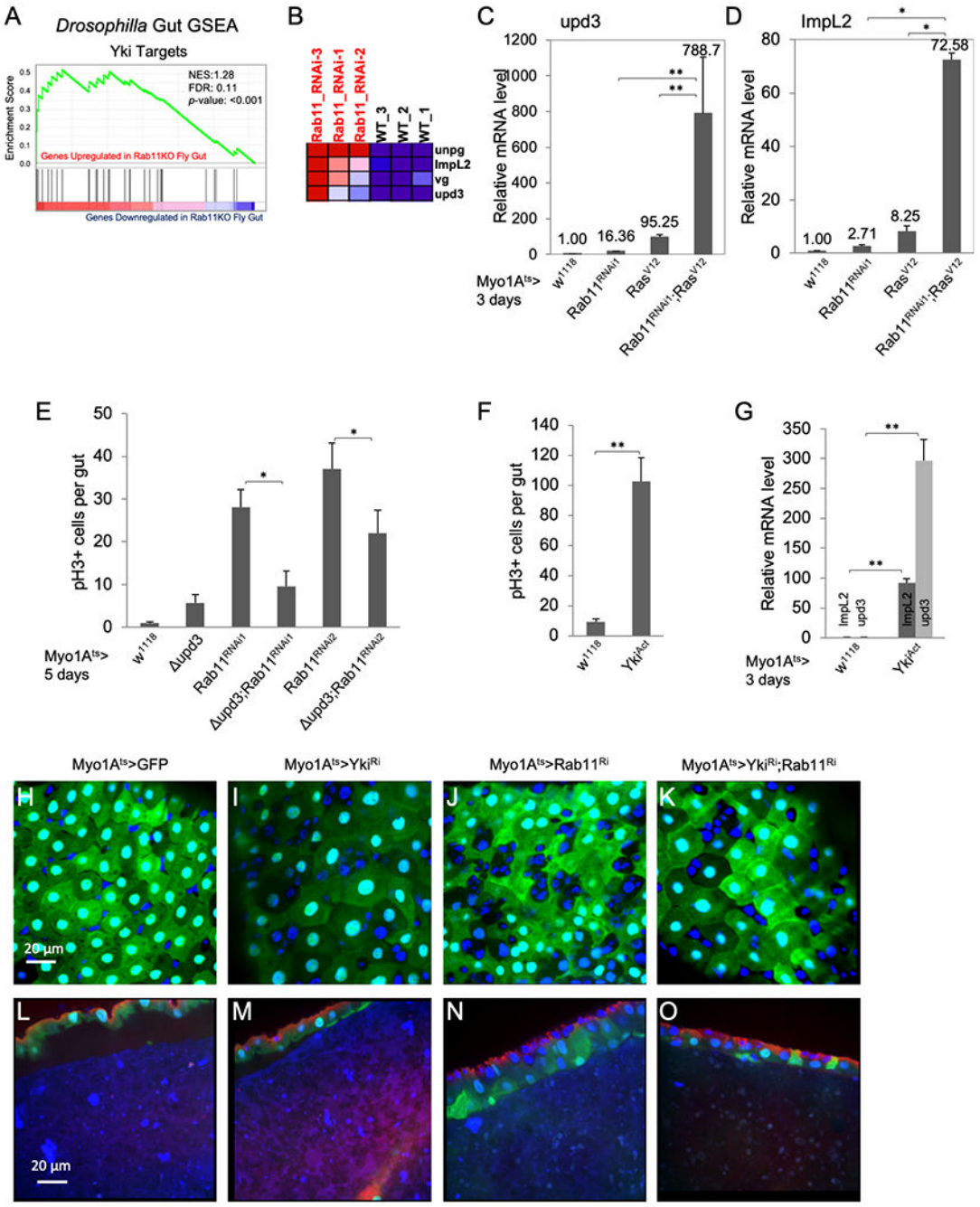

Fig. 6. *Drosophila* Yki regulates gene expression and midgut proliferation downstream of Rab11.

(A) GSEA was conducted to compare RNA samples isolated from midguts of UAS-Rab11 RNAi expressing flies and midguts of driver crossed with w^{1118} flies. Three independent RNAseq preps were used for this analysis.

(B) Schematic showing the 4 most elevated genes in Rab11 RNAi midguts.

(C) Quantitative PCR, from 3 independent experiments, of total RNA isolated from adult midguts using the *upd3* primers. Results were normalized relative to *rp49* qPCR from control flies of Gal4 driver crossed with the w^{1118} flies (see Materials and Methods).

(D) qPCR results using the *ImpL2* primers.
(E & F) Mitotic p-H3 counts from immunostained adult midgut samples. The Δ*upd3* is a null deletion mutant allele and homozygous flies were used following a 5-day 29°C temperature shift. * = p value<0.05.
(G) Quantitative PCR of total RNA from adult guts with the genotypes as indicated. Primers for *ImpL2* and *upd3* were used and compared to the control *rp49* in parallel PCR (see Materials and Methods for details).
(H) Flies were aged for 5-7 days and shifted to 29°C for 5 days to allow Gal4 driven transgenic expression. Guts were dissected and enterocytes were examined by confocal microscopy GFP and DAPI. Small nuclei that have no surrounding GFP are precursor cell nests.
(I) Confocal image of midgut expressing GFP from flies expressing yki-RNAi.
(J) Confocal image of midgut from flies expressing GFP and Rab11-RNAi. Precursor cell nests have more nuclei.
(K) Confocal image of midgut expressing GFP and both Rab11-RNAi and yki-RNAi.
(L) Longitudinal sagittal confocal micrograph of a posterior midgut from control fly showing the normal single-cell layered epithelium.
(M) Similar sagittal image to Panel L from GFP and yki-RNAi expressing fly.
(N) Sagittal view of midgut from fly expressing GFP and Rab11-RNAi; note the presence of the multi-layered epithelium.
(O) Confocal image of sagittal section of a midgut expressing GFP and both Rab11-RNAi and yki-RNAi; note the presence of a single-cell layered epithelium.

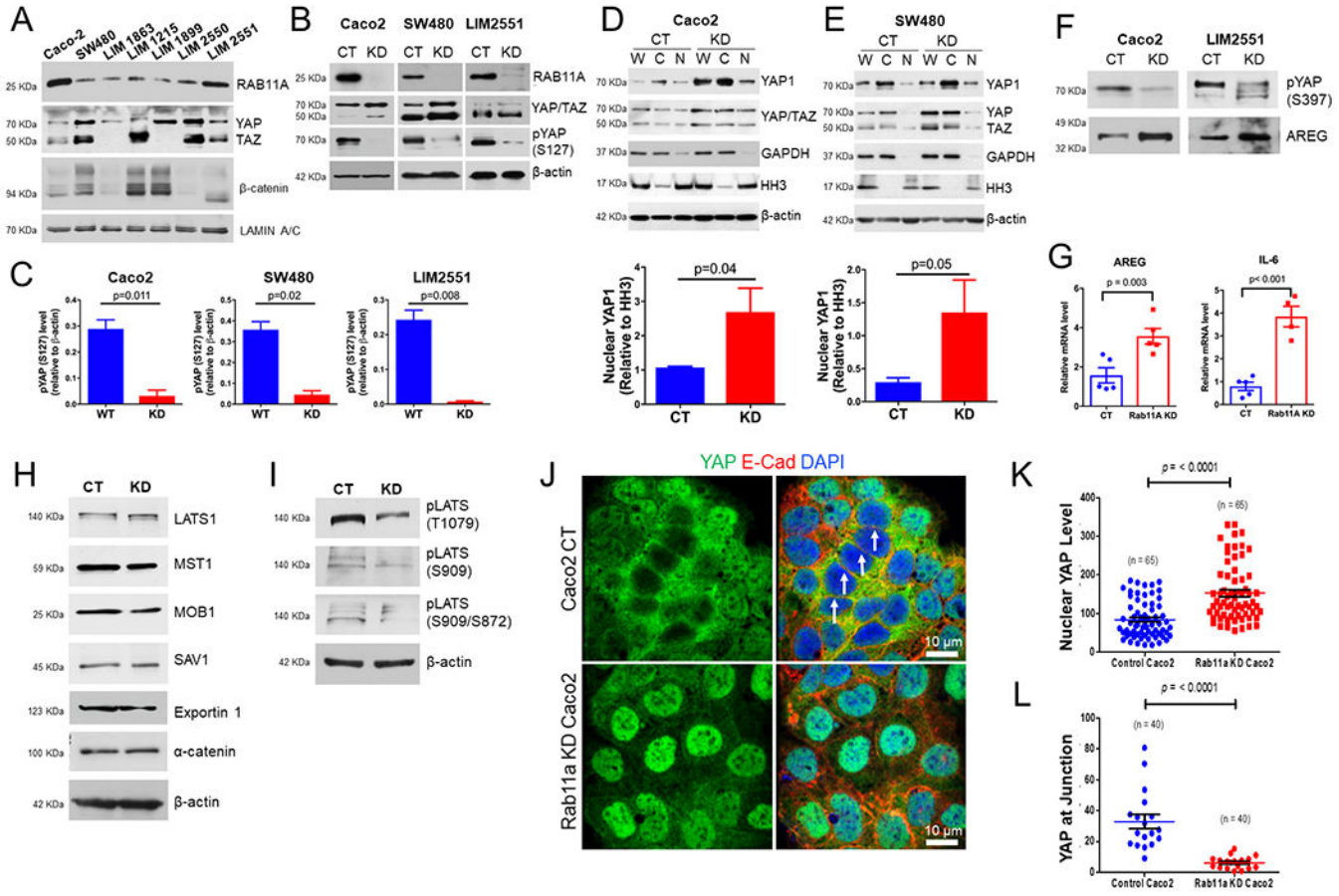

Figure 7. RAB11 supports LATS activity for YAP suppression.

(A) Western blot examiningf YAP expression in 7 human colon cancer cell lines.

(B) Rab11a KD reduced pYAP(S127) levels in Caco2, SW480, and LIM2551.

(C) pYAP (S127) levels are dramatically reduced in Rab11a KD cells. n=3 independent experiments.

(D-E) Two independent anti-Yap antibodies validated the increased nuclear Yap levels in Rab11a-KD Caco2 and SW480 cells in cell fractionation assays (3 independent experiments).

(F) Rab11a-KD Caco2 and LIM2551 cells show reduced pYAP(S397) and increased AREG levels.

(G) Quantitative RT-PCR shows increased AREG and IL-6 levels in RAB11A-KD Caco2 cells.

(H) Western blots show equivalent levels of Hippo kinase complex components, Exportin 1 and α-catenin in RAB11A-KD and control cells.

(I) Western blots show reduced phosphorylated LATS levels at T1079, S909, S872 in RAB11A-KD cells.

(J) Immunofluorescent staining shows the localization of a pool of Yap at cell-cell junctions in control cells (arrows). The junctional localization is reduced in RAB11A-KD cells. (K, L)

Quantification of fluorescence show significantly increased nuclear Yap levels and decreased Yap at junctions.

KEY RESOURCES TABLE

REAGENT or RESOURCE	SOURCE	IDENTIFIER
Antibodies		
Rabbit anti -YAP (clone D8H1X)	Cell Signaling	14074, RRID: AB_2650491
Rabbit anti -YAP1 antibody	Abcam	ab52771, RRID:AB_2219141
Rabbit anti - YAP S127	Cell Signaling	4911S, RRID:AB_2218913
Rabbit anti - YAP S397	Cell Signaling	13619, RRID:AB_2650554
Rabbit anti - pERK	Cell Signaling	9101
Rabbit anti - β- catenin (clone D10A8)	Cell Signaling	D10A8, RRID:AB_11129256
Rabbit anti - Rab11a	US Biological	R0009, RRID:AB_2284621
Rabbit anti - Rab11b	Sigma Aldrich	HPA054396, RRID:AB_2682474
Rabbit anti - Olfm4 (clone D6Y5A)	Cell Signaling	39141, RRID: AB_2650511
Rabbit anti – YAP/TAZ (D24E4)	Cell Signaling	8418, RRID:AB_10950494
Rabbit anti - Ki67 (clone SP6)	Abcam	ab16667, RRID:AB_302459
Rabbit anti - Histone H3 (clone D1H2)	Cell Signaling	4499, RRID:AB_10544537
Rabbit anti – GAPDH (clone 14C10)	Cell Signaling	3683, RRID:AB_1642205
Rabbit anti - Phospho-Stat3 (Y705) (clone D3A7)	Cell Signaling	9145, RRID: AB_2491009
Rabbit anti - Phospho-LATS1 (Ser909)	Cell Signaling	9157, RRID:AB_2133515
Rabbit anti - Phospho-LATS1 (Thr1079) (clone D57D3)	Cell Signaling	8654S, RRID:AB_10971635
Rabbit anti - Phospho-LATS1/LATS2 (Ser909, Ser872)	Invitrogen	PA5–64591, RRID:AB_2664907
Rabbit anti - LATS1 (Clone C66B5)	Cell Signaling	3477, RRID:AB_2133513
Rabbit anti – MOB1	Cell Signaling	3863S, RRID:AB_2087851
Rabbit anti - MST1	Cell Signaling	3682S, RRID:AB_10694384
Rabbit anti – SAV1(D6M6X)	Cell Signaling	13301
Rabbit anti - Exportin-1/CRM1 (D6V7N)	Cell Signaling	46249
Mouse anti – Rab11	BD Biosciences	610657, RRID:AB_397984
Mouse anti -E-Cadherin (clone 36/E-Cadherin)	BD Biosciences	610182, RRID: AB_397581
Mouse anti - AREG/amphiregulin	Santa Cruz Biotechnology	sc-74501, RRID:AB_1118939
Mouse anti – YAP1 (clone 2F12)	Novus Biologicals	H00010413-M01, RRID: AB_10694607
Mouse anti C- Myc (9E10)	Santacruz	sc-40, RRID:AB_627268
Mouse anti - PCNA (clone CP10)	Santa Cruz Biotechnology	sc-56, RRID: AB_628110
Mouse anti –pan-Cytokeratin (AE13)	Abcam	ab27988, RRID:AB_777047
Mouse anti - Lamin A/C (E-1)	Santa Cruz Biotechnology	sc-376248, RRID:AB_10991536
TO-PRO-3 Iodide (642/661)	Invitrogen	1830263
4′,6-Diamidino-2-Phenylindole (DAPI)	Santa Cruz	SC3598
Donkey anti-Rabbit, Alexa Fluor 488	Thermo Fisher Scientific	A-21206
Donkey anti-Rabbit, Alexa Fluor 546	Thermo Fisher Scientific	A10040
Donkey anti-Mouse, Alexa Fluor 555	Thermo Fisher Scientific	A-31570
Biotinylated Horse Anti-Mouse IgG Antibody	Vector Laboratories	BA-2000

REAGENT or RESOURCE	SOURCE	IDENTIFIER
Biotinylated Horse Anti-Rabbit IgG Antibody	Vector Laboratories	BA-1100
Reagents used		
VECTASTAIN Elite ABC HRP Kit (Peroxidase, Standard)	Vector Laboratories	PK-6100
DAB Peroxidase (HRP) Substrate Kit (with Nickel), 3,3'-diaminobenzidine	Vector Laboratories	SK-4100
RNeasy Plus Micro kit	Qiagen	74034
IntestiCult™ Organoid Growth Medium	STEMCELL Technologies	06005
Chemicals or Reagents		
Citric acid	Sigma-Aldrich	251275
Donkey serum	Sigma-Aldrich	D9663
Bovine Serum Albumin	Sigma-Aldrich	A3294
Advanced DMEM/F12 medium	Thermo Fisher Scientific	12634028
SignalStain EDTA Unmasking Solution (10X)	Cell Signaling	14747
Sepharose A/G beads	Santa Cruz Biotechnology	sc - 2003
Matrigel	Corning	356231
(Z)-4-Hydroxytamoxifen (4-OHT)	Sigma	H7904
Corning Recovery Solution	Corning	354253
IntestiCult Ogranoid Growth medium	StemCell Technologies	06005
DAKO target retrieval solution 10X concentrate	Agilent	S1699
Cytoseal 60	Thermo Scientific	83104
Prolong Gold antifade medium	Thermo Fisher Scientific	P36930
Experimental Models: Organisms/Strains		
$Rab11a^{flox}$		(Yu et al., 2014a)
APC^{Min}		*(Moser et al., 1990)*
Villin-CreER		(el Marjou et al., 2004)
Villin-Cre		(Madison et al., 2002)
Rab11b-null		This paper
Oligonucleotides		
IL-6 (Human) Forward, 5' – AAGCCAGAGCTGTGCAGATG – 3' and reverse 5'-TGGGTCAGGGGTGGTTATTG – 3'		
IL-6 (Mouse) Forward, 5' - AAATTTCCTCTGGTCTTCTGGAG – 3' and reverse, 5'- CGCACTAGGTTTGCCGAGTA- 3'		
AREG (Human) Forward, 5' – CGGGAGCCGACTATGACTAC – 3' and reverse, 5' GGGGGCTTAACTACCTGTTCA – 3'		
Areg (Mouse) Forward, 5' – GCATCGGCATCGTTATCACA – 3' and reverse, 5'-TCCCGTTTTCTTGTCGAAGC- 3'		
β – actin (Human) Forward, 5' – GCACAGAGCCTCGCCTTT – 3' and reverse, 5' – GAAGCCGGCCTTCGCACAT – 3'		
Hprt (mouse): Forward, 5'-TCCCTGGTTAAGCAGTACAGC-3' and reverse, 5'- TCCAACAAAGTCTGGCCTGT-3'		